

PACS numbers: 61.72.Uj, 71.55.Eq, 78.40.Fy, 82.30.Lp

THE IMPURITY ION INFLUENCE ON THE OPTICAL AND PHOTOCATALYTIC PROPERTIES OF ANATASE AND RUTILE

V. Shymanovska¹, L. Kernazhitsky¹, G. Puchkovska¹, V. Naumov¹,
T. Khalyavka², V. Kshnyakin³, S. Kshnyakina³, V. Chernyak⁴

¹ Institute of Physics, National Academy of Sciences of Ukraine,
46, Nauki Prosp., 03028 Kiev, Ukraine
E-mail: kern@iop.kiev.ua

² Institute for Sorption and Problems of Endoecology,
National Academy of Sciences of Ukraine,
13, Gen. Naumov Str., 03164 Kiev, Ukraine

³ Sumy State Pedagogical University,
87, Romens'ka Str., 40002 Sumy, Ukraine

⁴ Taras Shevchenko National University,
2/5, Acad. Glushkova Prosp., 03122 Kiev, Ukraine

The influence of Cu, Fe, Co, and Cr transition metal ion impurities on the optical absorption spectra of polydisperse powders of nanocrystalline TiO₂ rutile and anatase synthesized in identical experimental conditions is studied. For all rutile samples, no spectral shift of the absorption edge is observed, while a significant red shift of the absorption edge for modified anatase is detected. The shift value correlates well with the relative position of the impurity levels in the TiO₂ band gap. The effect of the impurities on the rutile optical absorption is observed only in the region 3,0-4,5 eV, whereas the modified anatase absorption changes significantly in the region 3,0-5,5 eV. The band gap remains practically unchanged for modified rutile, whereas it decreases for modified anatase, being the largest for A/Cr and A/Fe samples. The photocatalytic activity of rutile and anatase samples in the reaction of photodestruction of organic dye safranin under UV irradiation is investigated. It is shown that the transition metal impurities in rutile, at their high concentration, become additional recombination centers for photoexcited electron-hole pairs that leads to the inhibition of photocatalysis. Increase in the rate of photocatalysis in the presence of modified anatase correlates well with the increasing optical absorption of modified anatase in the region 4,0-5,5 eV.

Keywords: TITANIUM DIOXIDE, ANATASE, RUTILE, TRANSITION METAL IMPURITIES, OPTICAL PROPERTIES, PHOTOCATALYSIS.

(Received 25 January 2011, in final form 09 March 2011, online 03 April 2011)

1. INTRODUCTION

Titanium dioxide exhibits interesting optical properties, such as high transparency in the visible spectrum range, high index of refraction (2,4-2,7), band gap width of TiO₂ is equal to 3,0-3,2 eV depending on the crystalline structure. These properties allow to efficiently use TiO₂ in photocatalysis, solar cells, sensors, and for photon crystals. But wide band gap of TiO₂ allows to activate it only in the ultraviolet (UV) light that restricts the possible applications.

Many investigations have been carried out concerning the influence of different impurity atoms and compounds on the electron and optical properties of TiO_2 for the purpose of the improvement of these properties and extension of TiO_2 operating range to the visible spectrum region [1-3]. Anpo et al. [1] have shown that implantation of transition metal ions into TiO_2 shifts its optical absorption edge toward lesser energies. In spite of a large amount of publications devoted to the effect of impurities on the optical and electron properties of TiO_2 , it is quite difficult to make a direct comparison between the experimental results of different authors because of different conditions of TiO_2 synthesis and experimental techniques. Synthesis conditions, thermal and chemical treatment of TiO_2 , type and concentration of impurities are the determinative parameters in the given case.

The aim of this work was to investigate the influence of Cu, Fe, Co, Cr transition metal impurities on the optical and photocatalytic properties of polydisperse nanocrystalline TiO_2 of rutile (R) and anatase (A) modification with a high degree of chemical purity synthesized in the same experimental conditions. Optical absorption of TiO_2 samples were studied in a wide UV and visible spectrum range from 220 to 730 nm (in the photon energy region of 1,75-5,5 eV). Photocatalytic activity of the samples was investigated in the reaction of photodestruction of organic dye safranin under UV irradiation in the region of 254 nm. The obtained experimental results are presented and discussed in the given work.

2. EXPERIMENT

2.1 Materials

Polydisperse pure titanium dioxide with nanocrystalline structure of rutile or anatase was synthesized by thermal hydrolysis of TiCl_4 chloride solutions in the presence of colloidal nucleuses of anatase or rutile [4]. This method allows to obtain high purity TiO_2 with impurity (Cu, Fe, Co, Cr, Mn, V, Ni) content of 10^{-5} - 10^{-6} mas%. Then obtained samples of nanocrystalline anatase or rutile were modified by separate transition metal ions Cu^{2+} , Fe^{2+} , Co^{2+} , Cr^{3+} by adsorption from dilute aqueous solutions of the corresponding salts at pH = 7-8. Adsorption of impurity cations was performed during 24 hours to achieve the sorption equilibrium. Then samples were filtered out, dried at the temperature of 120°C, thoroughly washed by bidistilled water (until total absence of impurity ions in filtrate), and dried in the air at the temperature of 300°C. Samples for optical investigations were produced as compressed to a tablet TiO_2 and KBr powder mixtures (TiO_2 content was equal to 0,1%).

2.2 Investigation methods

Structural properties and phase composition of TiO_2 samples were studied by the X-ray diffractometry (XRD) method on the diffractometer DRON-2 with $\text{Cu}_{K\alpha}$ radiation ($\lambda = 0,154$ nm). Chemical composition of the samples was investigated by the method of the X-ray fluorescence analysis (XRF) using the device XNAT-Control. The scanning electron (SEM) microscope JEOL JSM 6490 with X-ray spectrometer was used to explore the surface morphology and for elemental analysis of the samples. SEM images and energy-dispersion spectra (EDS) were obtained at the voltage of 20 kV.

Optical absorption spectra of TiO₂ samples in the UV and visible spectrum range (in the wavelength range $\lambda = 220\text{-}750$ nm) were studied using the multi-channel optical analyzer SOLAR SL40-2 (3648-pixel CCD-detector TCD1304AP, diffraction grating is 600 mm⁻¹, spectral resolution is 0,3 nm, operating speed is 7 ms) under control of portable PC. Deuterium lamp DDC-30 ($\lambda_{1\text{max}} = 245$ nm and $\lambda_{2\text{max}} = 311$ nm) and xenon lamp ($\lambda_{\text{max}} = 472$ nm) were used as the sources of UV and visible light, respectively. Measurements were performed in standard conditions at room temperature.

Photocatalytic activity of the samples was investigated using the model reaction of photocatalytic destruction of organic dye safranin (C₂₀H₁₉ClN₄: H₂O solution) in a quartz reactor under the action of UV irradiation of the mercury lamp BUV-30 ($\lambda_{\text{max}} = 254$ nm, power 30 W). Changes of the safranin concentration in solution in certain time intervals were determined using absorption spectrophotometer SPECORD 20 UV-VIS.

3. RESULTS AND DISCUSSION

3.1 Structural and elemental analysis of TiO₂ samples

Structural characteristics of the investigated TiO₂ samples are presented in Table 1. In conformity with the XRD analysis results, average nanocrystal sizes in polydisperse TiO₂ powders are equal to 10-36 nm for rutile and 8-16 nm for anatase.

Table 1 – Characteristics of the synthesized TiO₂ samples

TiO ₂ samples	Impurity content, at% (XRF)*	Impurity content, at% (XRF)**	Impurity content, at% (EDS)**	Crystal grain size, nm (XRD)	Cell parameter <i>a</i> , Å (XRD)	Cell parameter <i>c</i> , Å (XRD)
RUTILE						
R	–	–	–	21	4,591	2,968
R/Cr	2,8	1,0	2,3	36	4,591	2,968
R/Co	7,0	2,4	1,1	29	4,564	2,981
R/Fe	6,3	2,2	3,5	15	4,550	3,000
R/Cu	12,5	4,5	4,6	10	4,553	3,026
ANATASE						
A	–	–	–	16	3,775	9,402
A/Cr	7,5	2,6	–	15	3,775	8,983
A/Co	9,3	3,3	–	13	3,781	9,099
A/Fe	7,5	2,6	–	9	3,787	9,015
A/Cu	15,3	5,7	–	8	3,793	9,343

* per one Ti atom;

** per one atom of TiO₂ compound.

Impurity ion content in synthesized samples was estimated using the XRF and EDS analysis methods. Elemental composition of the samples (content of Ti atoms, impurity ions, oxygen as well) was determined by the EDS data. Results of EDS for modified rutile were obtained using microprobe analysis realized in different surface points of TiO₂ particles. We have to note that by the XRF data, impurity concentrations are calculated per total amount of

Ti atoms, while EDS is based on total amount of Ti atoms, impurity atoms, and oxygen. Results of the XRF analysis were re-calculated per total atomic content in TiO_2 for the comparison with the EDS data.

Based on the XRF and EDS data, an arrangement of impurity cations in rutile samples is analyzed. Thus, Cu atoms are uniformly distributed both in the particle volume and on the surface; Cr and Fe atoms are more segregated on the surface of TiO_2 particles, and Co atoms are more incorporated to the particle volume. By the EDS data, content of Cr and Fe atoms in rutile is 1,5-2 times more than by the XRF data. Such distribution of Cr and Fe atoms on the surface and in the volume of TiO_2 particles is explained by their low solubility (the limit is about 1 mas%) in TiO_2 [5]. We have to note, content of Co ions on the surface of TiO_2 particles is substantially less than in the volume. This is conditioned by high diffusion coefficient of Co atoms from the surface into TiO_2 volume, which is observed even at low temperatures [6].

3.2 Structural and elemental analysis of TiO_2 samples

Optical absorption spectra measured in the range of photon energies from 1,75 to 3,1 eV for the samples of pure and modified TiO_2 rutile and anatase are shown in Fig. 1a, b in the form of the absorption coefficients α .

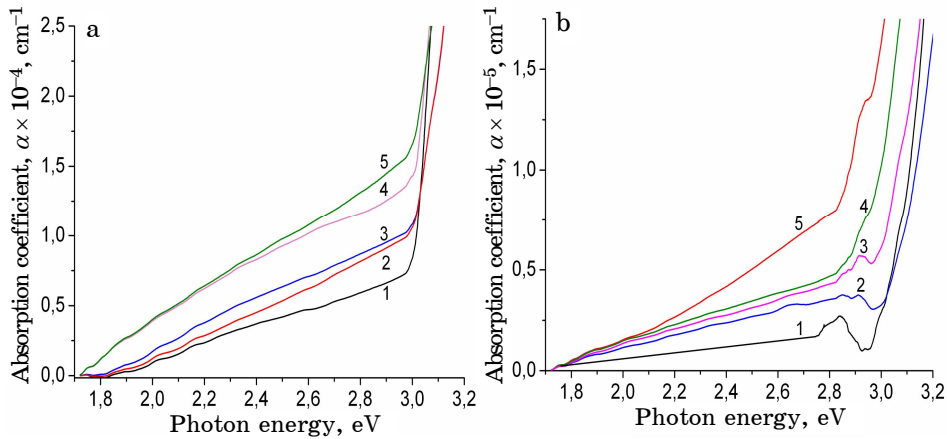


Fig. 1 – Absorption spectra of pure and modified TiO_2 in the range of 1,75-3,1 eV: 1 – R, 2 – R/Cr, 3 – R/Cu, 4 – R/Co, 5 – R/Fe (a) and 1 – A, 2 – A/Cu, 3 – A/Co, 4 – A/Fe, 5 – A/Cr (b)

For pure TiO_2 in the energy region from 2,0 to 3,0 eV one can observe a weak absorption induced by optical transitions between the states positioned above the top of the valence band (VB) and lower the bottom of the conduction band (CB). As known, these states are connected with bulk and surface defects and can be populated due to thermal excitation of CB electrons even at room temperature [7]. Increase in the absorption observed for the samples of modified TiO_2 can be connected with both the appearance of additional impurity states in the band gap and the intrinsic absorption of impurity atoms. These additional states are located above the top of the VB on 0,35 eV for Cr [7, 8] and 0,2 eV for Fe [2], on the top of the VB for Co [2], and within the BG for Cu [8], and all transitions lead to the sp-d charge transfer from these states to the CB of Ti^{4+} .

Obtained TiO₂ absorption spectra have the following peculiarities.

1. For all samples of modified anatase A/Co, A/Fe, and A/Cr (excluded A/Cu), substantial red shift of the absorption edge in the range 2,7-3,1 eV in comparison with pure anatase is observed. This shift correlates with the relative position of impurity levels in the TiO₂ band gap. The most expressed red shift is observed for A/Cr. Absorption peak near 2,80-2,85 eV (Fig. 1b) is connected with the increase in structural defects of anatase in comparison with rutile.

2. For all samples of rutile, in contrast to anatase, shift of the absorption edge is not observed. Absence of this shift implies that adsorption of impurities on rutile does not lead to the appearance of additional states in the TiO₂ band gap.

3. Absorption coefficients for rutile samples decrease as $R < R/Cr < R/Cu < R/Co \leq R/Fe$, and for anatase ones as $A < A/Cu < A/Co < A/Fe < A/Cr$.

4. Absorption curves for R/Fe and R/Co have almost the same behavior (Fig. 1a and Fig. 1b). This is connected with the fact that concentrations of Fe²⁺ and Co²⁺ impurity ions in these samples are almost equal, cations have identical ion radiuses and close intrinsic absorption bands (1,9-3,1 eV [5, 9] and 2,25-3,1 eV [10], respectively).

5. As for a small absorption for R/Cr, this is connected with low concentration of Cr³⁺ ions in rutile in comparison with other impurities. Large absorption for A/Cr is connected with the increase in the concentration of Cr³⁺ ions in anatase (Table 1) and strong intrinsic absorption of Cr at 2,0 eV [11-13] and 2,65 eV [14]. This corresponds to the transitions with charge transfer $Cr^{3+} \rightarrow Ti^{4+}$ and $4A_{2g} \rightarrow 4T_{1g}$ in octahedral environment [15].

6. Though concentration of Cu²⁺ ions in A/Cu and R/Cu samples was the largest, absorption of these samples in the range 1,8-3,0 eV is the lowest. This is explained by the fact that intrinsic absorption of Cu is shifted to the region 2,81-3,87 eV [16] in comparison with other impurities.

Absorption spectra measured in the range of photon energies from 2,7 to 5,5 eV for samples of pure and modified TiO₂ rutile and anatase are shown in Fig. 2a, b. As seen, the influence of impurities on absorption is stronger expressed for anatase than for rutile, but the main laws are similar for all samples.

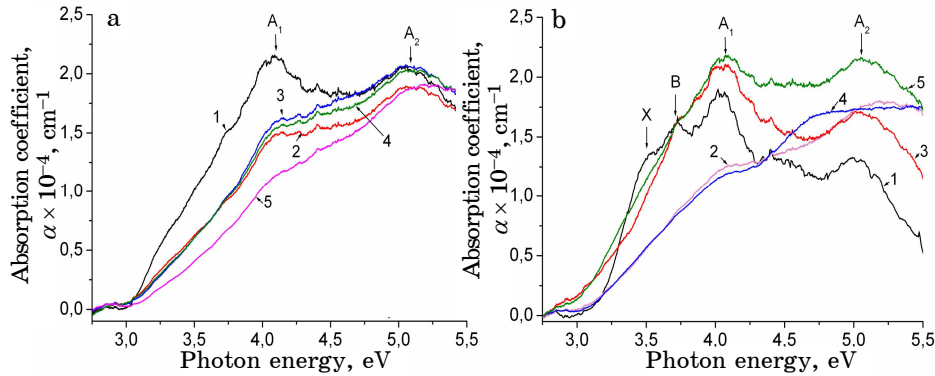


Fig. 2 – Absorption spectra of pure and modified TiO₂ in the range 2,7-5,5 eV: 1 – R, 2 – R/Cr, 3 – R/Cu, 4 – R/Fe, 5 – R/Co (a) and 1 – A, 2 – A/Co, 3 – A/Cr, 4 – A/Cu, 5 – A/Fe (b)

Two absorption bands with maximums A_1 and A_2 are observed in both pure and modified rutile and anatase. These bands correlate well with the bands in absorption spectra of monocrystalline TiO_2 obtained experimentally [17] and calculated theoretically [18].

In absorption spectra of pure rutile (Fig. 2a) bands A_1 and A_2 are connected with the splitting of O $2p_{x,y}$ orbital of oxygen atoms in the VB [19, 20]. Band A_1 at 4,05 eV is connected with the transitions between upper edge of the VB and bottom of the CB (conditionally “first order” transitions). Band A_2 at 5,08 eV is related to the transitions between four upper valent states of the VB and first six states t_{2g} in the CB (“second order” transitions). In absorption spectra of pure anatase (see Fig. 2b) bands A_1 and A_2 are located close to 4,03 and 5,00 eV, respectively, and are the consequence of the transitions from the VB into the CB. Also, absorption bands X and B at 3,5 and 3,7 eV, respectively, are observed for pure anatase. Band B was observed earlier for anatase monocrystal at 3,6 eV [21], but we did not find any information elsewhere about band X. Asahi et al. [22] ascribed band B to $O^{2-} \rightarrow Ti^{4+}$ transitions with charge transfer. They have also shown that this transition is the dipole-forbidden at $E \parallel c$ polarization and is the dipole-allowed at $E \perp c$.

We should notice the following peculiarities of TiO_2 absorption spectra.

a) Impurities in rutile lead to the significant decrease in the absorption band A_1 and the increase in the band A_2 , and, as a consequence, to the redistribution of the absorption ratio in bands A_1 and A_2 . Minimum absorption of A_1 is observed for R/Co sample. Absorption ratio in bands A_1 and A_2 for rutile R : R/Cr : R/Cu : R/Co : R/Fe is changed as 1 : 0,8 : 0,8 : 0,8 : 0,7. This implies the increase in the relative intensity of the “second order” transitions, i.e. between upper valent states of the VB and t_{2g} states in the CB.

b) Impurities in anatase lead to complex changes in the relative absorption in bands A_1 and A_2 . Absorption of A_1 for doped anatase samples in comparison with pure anatase increases for A/Cr and A/Fe, but decreases substantially for A/Co and A/Cu. Absorption ratio A : A/Cr : A/Fe : A/Co : A/Cu in bands A_1 and A_2 is changed as 1,4 : 1,2 : 1,0 : 0,7 : 0,7. This implies the different effect of impurities on the electron transitions in anatase: relative intensity of the “first order” transitions increases for A/Cr and A/Fe and essentially decreases for A/Co and A/Cu. But for all samples of modified anatase relative intensity of the “second order” transitions substantially increases in comparison with pure anatase.

c) A wide background in the range 4,4-4,9 eV and shift of the band A_2 to the long-wave region in comparison with other anatase samples are observed on the absorption spectra of A/Cu. This occurs due to the overlap of the absorption bands, which correspond to $O^{2-}(2p) \rightarrow Ti^{4+}(3d)$ and $O^{2-}(2p) \rightarrow Cu^{2+}(3d)$ transitions with charge transfer [23].

3.3 Band gap width

Band gap width E_g of semiconductors is connected with the absorption coefficient α and can be determined from equation [24]

$$A (h\nu - E_g)^r = \alpha h\nu, \quad (1)$$

where $h\nu$ is the photon energy; A is the constant, which correlates with the ordering of the crystal structure; $r = 2$ for indirect allowed transitions; $r = 3/2$

for direct forbidden transitions, and $r = 1/2$ for direct allowed transitions. Band gap width of TiO₂ rutile and anatase samples was defined by the intersection of tangent $(\alpha h\nu)^{1/r}$ to the photon energy axis as it is shown in Fig. 3 and Fig. 4, respectively.

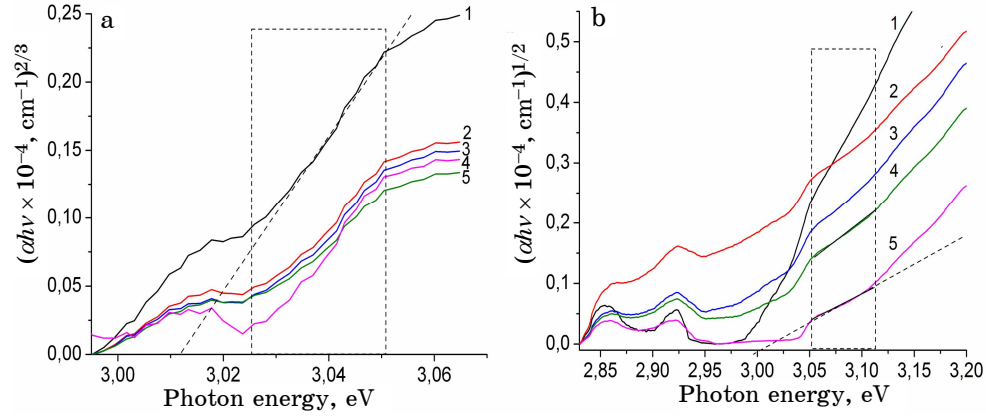


Fig. 3 – Dependence of $(\alpha h\nu)^{1/r}$ on the photon energy for pure and modified rutile:: 1 – R, 2 – R/Cr, 3 – R/Cu, 4 – R/Co, 5 – R/Fe (a) and 1 – R, 2 – R/Cr, 3 – R/Cu, 4 – R/Fe, 5 – R/Cr (b)

Obtained values of the band gap width of direct E_{gd} and indirect E_{gi} transitions for polycrystalline rutile samples in comparison with the references are represented in Table 2.

Table 2 – Values of the band gap width for rutile samples

Samples	E_{gd} , eV $r = 1,5$	E_{gi} , eV $r = 2$	E_g , eV taken from the references (impurity content, %)	References
R	3,01	2,97	3,0	[29]
R/Fe	3,02	2,83	2,8 (1 at.%)	[29]
R/Cr	3,02	2,91	3,25 (1 at.%); 3,15(10 at.%)*	[30]
R/Co	3,03	2,99	2,72 (3 at.%)*	[31]
R/Cu	3,02	2,93	3,00 (0,5 M.%); 3,06 (1,0 M.%)	[32]

* data for TiO₂ films.

For the samples of pure rutile we have found the band gap width of direct transitions: $E_{gd} = 3,01$ eV. This value agrees well with the data for rutile monocrystal [27] and it was discussed in our previous work [28]. As follows from the experimentally obtained data, for modified rutile samples, in comparison with pure rutile, band gap width remains practically unchanged.

Energy states in the band structure of anatase, in contrast to rutile, have two maximums in the upper region of the VB, and difference in the energies between these two maximums is very small (0,1 eV) [22, 33]. Electron transition from these maximums to the bottom of the CB can be both direct Γ (VB) \rightarrow Γ (CB) [22] and indirect M (VB) \rightarrow Γ (CB) [33]. What this transition is – direct or indirect – this completely depends on the crystal structure, lat-

tice parameters, and dispersed composition of semiconductor. Though monocrystalline TiO_2 is an indirect semiconductor, TiO_2 -based nanostructured materials can exhibit properties of “direct” semiconductors [34, 35].

Starting from our experimental data, for polydisperse anatase samples we have determined the band gap width for two types of transitions: direct and indirect. In Fig. 4 we show the dependences $(\alpha h\nu)^{1/r}$ on $h\nu$ for anatase, which correspond to the direct and indirect transitions at $r = 2$ (a) and $r = 0,5$ (b), respectively.

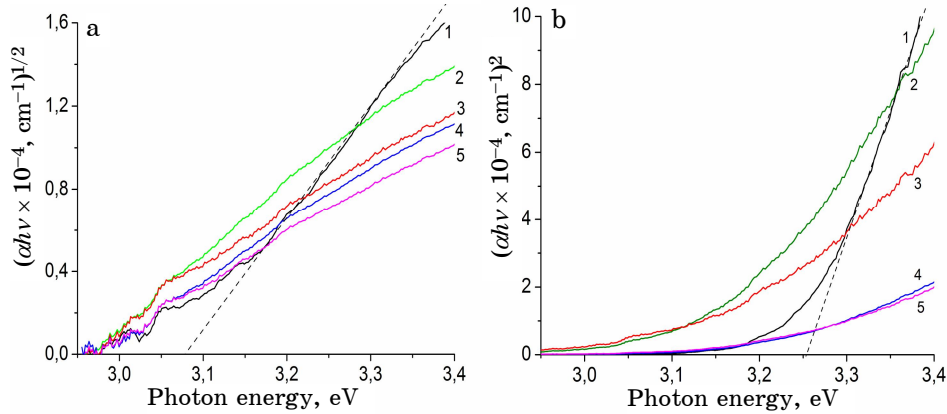


Fig. 4 – Dependence of $(\alpha h\nu)^{1/r}$ on the photon energy for pure and modified anatase: 1 – A, 2 – A/Fe, 3 – A/Cr, 4 – A/Cu, 5 – A/Co (a) and 1 – A, 2 – A/Fe, 3 – A/Cr, 4 – A/Cu, 5 – A/Co (b)

Obtained values of the band gap width of direct E_{gd} and indirect E_{gi} transitions for polycrystalline anatase samples in comparison with the references are represented in Table 3.

Table 3 – Values of the band gap width for anatase samples

Samples	E_{gd} , eV $r = 0,5$	E_{gi} , eV $r = 2$	E_g , eV taken from the references (impurity content, %)	References
A	3,25	3,08	3,22; 3,19; 3,45; 3,29*	[36][37][32][39]
A/Cr	3,14	2,94	–	–
A/Cu	3,21	2,97	3,15 (0,5 M.%); 3,37 (1,0 M.%)	[32]
A/Co	3,20	2,94	3,26-2,53 (0-35%)* 3,14 (4 at.%), 2,96*(7 at.%)	[38] [37]
A/Fe	3,13	2,96	2,88 (4,89 at.%) 2,83 (25 at.%)* 3,15 (2 at.%)	[9] [39] [37]

* data for TiO_2 films.

We have found some papers connected with indirect band gap for polydisperse TiO_2 , and only the authors of [9] represented data for direct band gap of anatase. In the cases when we have not found data for TiO_2 powders, data for TiO_2 films was taken.

Obtained value of the band gap width for direct transitions in pure anatase $E_{gd} = 3,25$ eV agrees well with the data of [36, 37] for TiO_2 with the same particle size as in our samples. Our estimation of the direct band gap for A/Cu and A/Fe also correlates well with the data of [32, 37] for anatase with the same particle size and impurity concentration.

3.4 Photocatalytic activity

Reaction of photodestruction of organic dye safranin under the action of UV irradiation ($\lambda_{\text{max}} = 254$ nm) was studied to estimate the photocatalytic activity of pure and modified anatase and rutile. In Fig. 5 we show the dependence of the relative safranin concentration in solution on the UV irradiation time.

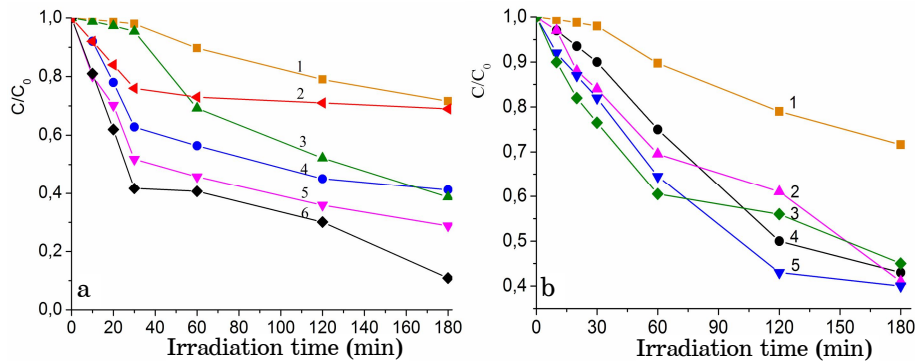


Fig. 5 – Photodestruction of safranin: (a) 1 – without catalyst, 2 – R/Cr, 3 – R/Fe, 4 – R/Cu, 5 – R/Co, 6 – R; (b) 1 – without catalyst, 2 – A/Co, 3 – A/Fe, 4 – A, 5 – A/Cu

In the absence of catalyst, photodecomposition of safranin is very slow, but the process is substantially accelerated in the presence of anatase or rutile, especially during first 30-60 minutes. The largest rate of safranin photodestruction was observed for pure rutile: in 30 minutes of UV irradiation almost 60% and in 180 min – about 90% of the dye are decomposed. Inhibition of photocatalytic reaction was observed for modified rutile. Modification by the transition metal cations of anatase, in contrast to rutile, leads to the increase in the reaction rate of safranin photodestruction. Thus, after 60 min of UV irradiation, relative concentration of safranin decreased: 25% for pure anatase, 30% for A/Co, 35% for A/Cu, 40% for A/Fe. Almost the same degree of dye photodecomposition (55-60%) was observed after 180 min of UV irradiation for all anatase samples.

Obtained results of the safranin photodestruction in the presence of TiO_2 correlate well with the data concerning the photoabsorption of anatase and rutile. As known, the rate of photocatalytic reaction depends on many factors: crystal size, specific surface of particles, impurity concentration, etc. Relation between the rate of photoinduced charge transfer from the volume to the surface of TiO_2 particle and the recombination rate of photoexcited electrons and holes plays an important role. Transition metal ion impurities, depending on their concentration, can be additional traps of photogenerated electrons and holes or be the centers of their recombination. There is an optimal concentration of the transition element impurities, above which these impurities act as the recombination centers [3].

Our experimental data shows that impurities in rutile (Fig. 5a) lead to the inhibition of safranin photodecomposition, because a large amount of these impurities leads to the appearance of additional recombination centers of the photoexcited electron-hole pairs. For anatase samples (Fig. 5b), inhibition of safranin photodecomposition due to the additional recombination centers is compensated by the increase in the rate of photocatalytic reaction because of the increase in the photoabsorption of modified anatase. Therefore, one can observe the correlation between the relative rate of photocatalysis and the relative coefficient of the optical absorption of anatase samples in the range 4,0-5,5 eV.

4. CONCLUSIONS

The influence of Cu, Fe, Co, and Cr transition metal ion impurities on the optical and photocatalytic properties of polydisperse powders of nanocrystalline TiO₂ of rutile and anatase modifications with a high degree of chemical purity synthesized in the same experimental conditions is studied in the present work.

Optical absorption spectra of pure and modified samples of anatase and rutile in a wide range of photon energies (1,75-5,5 eV) are investigated.

It is shown that in the region 2-3 eV absorption of TiO₂ is connected with optical transitions between defect states localized between the top of the VB and the bottom of the CB. Substantial increase in the absorption for all TiO₂ samples is conditioned by absorption of impurity ions.

Spectral shift of the absorption edge was not observed for all rutile samples, while significant red shift of the absorption edge, which correlates well with the position of impurity levels in the TiO₂ band gap, was registered for doped anatase samples (except of A/Cu).

Absorption of TiO₂ in the region 3,0-5,5 eV is conditioned by the electron transitions between the VB and t_{2g} states of the CB. Influence of impurities in rutile is observed only for the transitions in the region 3,0-4,5 eV, while absorption of doped anatase is substantially changed in the region 3,0-5,5 eV in comparison with pure anatase.

The band gap width of polydisperse TiO₂ samples is determined. It remains practically unchanged for doped rutile, whereas for doped anatase band gap width decreases being the largest for A/Cr and A/Fe samples.

Photocatalytic activity of TiO₂ samples in the reaction of photocatalytic decomposition of organic dye safranin under UV irradiation is studied. It is shown that for modified rutile the rate of photocatalytic reaction slows down because at large concentration of impurities they become the recombination centers of the photoexcited electron-hole pairs. On the contrary, for modified anatase acceleration of photocatalytic reaction is observed. Relative rate of photocatalysis in the presence of modified anatase correlates well with the relative coefficient of optical absorption of anatase samples in the region of 4,0-5,5 eV.

REFERENCES

1. M. Anpo, Y. Ichihashi, M. Takauchi, H. Yamashita, *Res. Chem. Intermediat.* **24**, 143 (1998).
2. T. Umebayashi, T. Yamaki, H. Itoh, K. Asai, *Appl. Phys. Lett.* **81**, 454 (2002).
3. O. Carp, C.L. Huisman, A. Reller, *Prog. Solid State Ch.* **32**, 33 (2004).

4. V. Shymanovska, A. Dvernyakova, V. Strelko, *Izv. AN SSSR. Neorg. Mat.* **24**, 1188 (1988).
5. C. Adan, A. Bahamonde, M. Fernandez-Garcia, A. Martinez-Arias, *Appl. Catal. B: Environ.* **72**, 11 (2007).
6. S.A. Chambers, S. Thevuthasan, R.F.C. Farrow, R.F. Marks, J.U. Thiele, L. Folks, M.G. Samant, A.J. Kellock, N. Ruzycski, D.L. Ederer, U. Diebold, *Appl. Phys. Lett.* **79**, 3467 (2001).
7. K. Mizushima, M. Tanaka, A. Asai, S. Iida, *J. Phys. Chem. Solids* **40**, 1129 (1979).
8. K. Ding, J. Li, Y. Zhang, *J. Mol. Struct. Theochem.* **728**, 123 (2005).
9. M. Asilturka, F. Saylkan, E. Arpac, *J. Photoch. Photobio. A* **203**, 64 (2009).
10. K. Das, Sh.N. Sharma, M. Kumar, S.K. De, *J. Phys. Chem. C* **113**, 14783 (2009).
11. E. Borgarello, J. Kiwi, M. Gratzel, E. Pelizzetti, M. Visca, *J. Am. Chem. Soc.* **104**, 2996 (1982).
12. N. Serpone, D. Lawless, J. Disdier, J.M. Herrmann, *Langmuir* **10**, 643 (1994).
13. L. Palmisano, V. Augugliaro, A. Sclafani, M. Schiavello, *J. Phys. Chem.* **92**, 6710 (1988).
14. R.C. da Silva, E. Alves, M.M. Cruz, *Nucl. Instrum. Meth. B* **191**, 158 (2002).
15. J.C. Yu, G. Li, X. Wang, X. Hu, Ch.W. Leung, Zh. Zhang, *Chem. Commun.* **2006**, 2717 (2006).
16. M. Iwamoto, H. Yahiro, N. Mizuno, W.X. Zhang, Y. Mine, H. Furukawa, S. Kagawa, *J. Phys. Chem.* **96**, 9360 (1992).
17. M. Cardona, G. Harbeke, *Phys. Rev.* **137**, 1467 (1965).
18. F.M. Hossain, L. Sheppard, J. Nowotny, G.E. Murch, *J. Phys. Chem. Solids* **69**, 1820 (2008).
19. J. Pascual, J. Camassel, H. Mathieu, *Phys. Rev. B* **18**, 5606 (1978).
20. K.M. Glassford, J.R. Chelikowsky, *Phys. Rev. B* **46**, 1284 (1992).
21. N. Hosaka, T. Sekiya, C. Satoko, S. Kurita, *J. Phys. Soc. Jpn.* **66**, 877 (1997).
22. R. Asahi, Y. Taga, W. Mannstadt, A.J. Freeman, *Phys. Rev. B* **61**, 7459 (2000).
23. H. Praliaud, Y. Kodratoff, G. Coudurier, M.V. Mathieu, *Spectrochim. Acta A* **30**, 1389 (1974).
24. J. Tauc, *Optical Properties of Solids* (North-Holland: Amsterdam: 1970).
25. H. Tang, H. Berger, P.E. Schmid, F. Levy, G. Burri, *Solid State Commun.* **87**, 847 (1993).
26. N. Daude, C. Gout, C. Jouanin, *Phys. Rev. B* **15**, 3229 (1977).
27. T. Umebayashi, T. Yamaki, H. Itoh, K. Asai, *J. Phys. Chem. Solids* **63**, 1909 (2002).
28. L. Kernazhitsky, V. Shymanovska, V. Naumov, V. Chernyak, T. Khalyavka, V. Kshnyakin, *Ukr. J. Phys. Opt.* **9**, 197 (2008).
29. L. Diamandescu, F. Vasiliu, D. Tarabasanu-Mihaila, M. Feder, A.M. Vlaicu, C.M. Teodorescu, D. Macovei, I. Enculescu, V. Parvulescu, E. Vasile, *Mater. Chem. Phys.* **112**, 146 (2008).
30. G.H. Takaoka, T. Nose, M. Kawashita, *Vacuum* **83**, 679 (2009).
31. N. Popovici, E. Jimenez, R.C. da Silva, W.R. Branford, L.F. Cohen, O. Conde, *J. Non-Cryst. Solids* **352**, 1486 (2006).
32. G. Colon, M. Maicu, M.C. Hidalgo, J.A. Navio, *Appl. Catal. B: Environ.* **67**, 41 (2006).
33. S. Mo, W.Y. Ching, *Phys. Rev. B* **51**, 13023 (1995).
34. N. Serpone, D. Lawless, V. Khairutdinov, *J. Phys. Chem.* **98**, 16646 (1995).
35. K.M. Reddy, S.V. Manorama, A.M. Reddy, *Mater. Chem. Phys.* **78**, 239 (2002).
36. H. Lin, C.P. Huang, W. Li, C. Ni, S.I. Shah, Y.H. Tseng, *Appl. Catal. B: Environ.* **68**, 1 (2006).
37. J.C. Colmenares, M.A. Aramendia, A. Marinas, J.M. Marinas, F.J. Urbano, *Appl. Catal. A: Gen.* **306**, 120 (2006).
38. W.B. Mi, E.Y. Jiang, H.L. Bai, *J. Magn. Magn. Mater.* **321**, 2472 (2009).
39. M.Ch. Wang, H.J. Linb, T.S. Yang, *J. Alloy. Compd.* **473**, 394 (2009).